



HAL
open science

Gas-phase polymerization of ultra-high molecular weight polyethylene with decreased entanglement density

Roberta Lopes Do Rosario, Fotis Christakopoulos, Theo Tervoort, Fabrice Brunel, Timothy Mckenna

► To cite this version:

Roberta Lopes Do Rosario, Fotis Christakopoulos, Theo Tervoort, Fabrice Brunel, Timothy Mckenna. Gas-phase polymerization of ultra-high molecular weight polyethylene with decreased entanglement density. *Journal of Polymer Science*, 2023, 10.1002/pol.20230038 . hal-04042860

HAL Id: hal-04042860

<https://hal.science/hal-04042860>

Submitted on 23 Mar 2023

HAL is a multi-disciplinary open access archive for the deposit and dissemination of scientific research documents, whether they are published or not. The documents may come from teaching and research institutions in France or abroad, or from public or private research centers.

L'archive ouverte pluridisciplinaire **HAL**, est destinée au dépôt et à la diffusion de documents scientifiques de niveau recherche, publiés ou non, émanant des établissements d'enseignement et de recherche français ou étrangers, des laboratoires publics ou privés.

Gas-phase polymerization of ultra-high molecular weight polyethylene with decreased entanglement density

*Roberta Lopes do Rosario, Fotis Christakopoulos, Theo A. Tervoort, Fabrice Brunel, and Timothy F. L. McKenna**

Dr. R. Lopes do Rosario

Dutch Polymer Institute DPI, P.O. Box 902, 5600 AX Eindhoven, The Netherlands

Dr. R. Lopes do Rosario, Dr. Fabrice Brunel, Dr. T. F. L. McKenna

CP2M UMR 5128, CNRS/UCBL/CPE-Lyon, 43 Blvd du 11 Novembre 1918, BP 2077,

69616 Villeurbanne, France

E-mail: timothy.mckenna@univ-lyon1.fr

Dr. F. Christakopoulos, Dr. T. A. Tervoort

ETH Zurich, Department of Materials, 8093 Zurich, Switzerland

Abstract: It is well known that ultra-high molecular weight polyethylene (UHMWPE) is a polymer with long chains and very high molecular weight, that poses difficulties in terms of processability due to the presence of chain entanglements. In many cases it is thus necessary to treat the material in different ways after the polymerization to minimize the amount of entanglements and improve the processability.

Based on observations that the use of inert condensing agents (ICA) had a noticeable impact on molecular weight and crystallinity, it was decided to develop a gas phase polymerization process with addition of ICA for UHMWPE with a high fraction of disentangled chains. For the optimization of this process, the comparison with slurry is important for the understanding of the improvement. Thus, a clear difference between slurry and gas phase is observed in terms of crystallinity and the lamellar thickness of the crystals, molecular weight and entanglements. Characterization techniques are developed to measure the properties of the reactor powder and understand the impact of the alkanes *in situ*. Using solid-state drawability, the entanglement degree of the reactor powder is analysed. From the SAXS and WAXS techniques, it is possible to find a correlation of entanglements and lamellar thickness. Moreover, crystallization kinetics measurements of the polymer in presence of ICA

constitutes a powerful method to explain the phenomena of entanglement and crystal formation.

Keywords: ultra-high molecular weight polyethylene; gas-phase polymerization; disentangled polyethylene; induced condensing agents; crystallization kinetics

1. Introduction

Ultra-high molecular weight polyethylene (UHMWPE) is a semicrystalline polymer, similar in structure to high density polyethylene (HDPE), with more robust properties including high impact strength, abrasion resistance, biocompatibility, low friction coefficient, high chemical and fatigue resistance, and chemical inertness. In terms of molecular weight, the definition of what constitutes UHMWPE appears to be somewhat arbitrary. ISO Standard 2304-1:2019 defines as a polyethylene with melt mass-flow rate (MFR) of less than 0.01 g min^{-1} measured at $190 \text{ }^\circ\text{C}$ and 21.6 kg load which gives a molecular weight of higher than 10^6 g mol^{-1} .^[1] In the other hand, ASTM D4020 defines it as a linear polyethylene with a relative viscosity (η_{rel}) higher than 1.44 at a concentration of 0.02% at 135°C in decahydronaphthalene, providing a molecular weight greater than $3.1 \times 10^6 \text{ g mol}^{-1}$.^[2] Celanese, one of the major UHMWPE manufacturers, considers that UHMWPE are resins with the molecular weight between 3.5×10^6 and $6 \times 10^6 \text{ g mol}^{-1}$.^[3] For the purpose of this paper, we will define UHMWPE as a polyethylene with molecular weight higher than $3 \times 10^6 \text{ g mol}^{-1}$.

UHMWPE reactor powders can be directly recrystallized and pressed to produce e.g. medical implants (hip and knee replacements), machined parts that wear better than steel, or as material in harbor construction.^[4] It can also be used in the form of high-performance UHMWPE fibers that are used in a wide range of high-end applications, including ballistic protection and cut-resistant garments, sails, and ropes. Such fibers have superior mechanical

properties owing to the almost complete orientation of the macromolecular chains.^[5–7] However, these superior properties are notoriously difficult to achieve due to the intractable nature of the starting materials. Unfortunately, most standard hexane slurry polymerization processes provide highly entangled product not directly suitable for ultra-drawing. Hence, it is not surprising that efficient processing routes or suitable starting materials for the production of high-performance polymer fibers are still being investigated.^[8] In order to reach the desired high values of tensile strength and modulus, a close-to-perfect macromolecular alignment is necessary, which is achieved by large-strain uniaxial solid-state plastic deformation, known as the so-called “ultra-drawing process”.^[9] For this process, a low-entangled UHMWPE fiber precursor is required, as the maximum draw ratio (λ_{\max}) in semi-crystalline polymers with weak interchain interactions drawn at elevated temperature, but below the melting temperature, is dictated by the entanglement density.^[10]

Low-entangled fiber precursors are typically achieved by starting from a dilute solution of UHMWPE in an organic solvent, like decalin, to reduce the entanglement density, followed by fixation of the low entanglement density through crystallization into a low-entangled gel and solvent evaporation, which is known as the so-called “gel-spinning” process.^[9–12] Even though this is the most commonly used process to industrially produce high strength and high modulus UHMWPE fibers, it requires the use of large amounts of toxic solvents. These solvents need impose strict working conditions, and have to be collected and recycled, increasing production cost and environmental impact. Solution polymerization on unsupported single site catalysts, such as metallocene catalysts, can produce highly disentangled UHMWPE when used in unsupported form since the chains formed this way are diluted enough that there are no chain-chain interactions.^[13] For instance, Rastogi and co-workers produce disentangled UHMWPE using an unsupported single site catalyst (phenoxyimine titanium complexes – FI catalyst) at low concentration and low temperature (i.e. below the crystallization temperature).^[14] Despite their many advantages, these types of

catalysts remain difficult to scale up from laboratory to production. The lack of a physical structure for creating polymer particles often results in severe reactor fouling.^[15] Therefore, a technology to produce low-entangled UHMWPE that provides control over the powder morphology is a desired target.

The first approach to directly synthesize UHMWPE with a low degree of using supported catalysts was demonstrated by Smith et al.^[16-18] They produced UHMWPE with a reduced number of entanglements using a, relatively low yield, vanadium Ziegler catalyst supported on a glass slide at a low reaction temperature (< 0 °C). In addition, the polymerization conditions necessary for the decreased entanglement density, lead to a very low polymerization rate that is economically unfavorable for industrial applicability. Recently, it has been shown that disentangled UHMWPE can be produced using a controlled reduction of Ti(IV) to Ti(III) by treating Mg-Ti catalyst with modified methylaluminoxane (MMAO12).^[19] Chamming et al. produced weakly entangled UHMWPE using a nano-dispersed MgO/MgCl₂/TiCl₄ catalyst and bulky alkyl aluminum for activation which increases the distance between the active sites.^[20] In all of these examples, the main strategies to obtain disentangled UHMWPE lie in the increased separation between active site and/or the decrease of their activities (and implicitly an increase in crystallization rate) often achieved by decreasing the temperature. However, these methods lack industrial significance and are only moderately successful in reducing the amount of entanglements. These examples were performed in slurry polymerization, as is currently the case for most industrial production. In slurry polymerization the diluents, which are typically short chain alkanes like propane, isobutane or hexane, are significantly less noxious than the solvents used for the gel-spinning process. Typically, two or three times the mass of product in terms of alkanes is needed in the process, and these products need to be purchased, removed and purified continuously.

A different approach to polymerizing ethylene for non-UHMWPE applications is in a gas-phase process with a supported catalyst. It has been recently shown that polyethylene

polymerized in gas phase in the presence of vaporized induced condensing agents (ICAs) significantly increases the crystallinity and provides molecular weight above 1500 kg mol⁻¹.^[21] In a companion work, these same authors also showed that using the same quantities of different alkanes led to the increase in the polymerization rate for heavier alkanes (i.e. the observed rate of polymerization in the gas phase was higher with n-hexane than with n-pentane).^[22] They attributed this to the so-called co-solubility effect. In the present work, refinements of the gas-phase polymerization of ethylene described in the work of Namkajorn et al.^[21] are explored as an alternative way to produce disentangled UHMWPE reactor powder for use in ultra-drawing processes, while retaining control over the powder morphology. Gas phase processes generally have lower capital and operating costs than slurry, but heat transfer can be more problematic. The main advantage with gas phase process here is that one can directly make UHMWPE with low degrees of entanglement in this process – something that is not possible in slurry.

Several polymerization conditions are investigated and the entanglement density of the resulting reactor powder is evaluated through solid-state drawability measurements. In an attempt to understand the mechanism behind the low entanglement of gas-polymerized UHMWPE and to steer further research, the effect of the different polymerization conditions together with the crystallization kinetics and the lamellar thickness of UHMWPE reactor powder are studied. Last, high-performance UHMWPE fibers are produced and compared with data from literature.

2. Slurry and gas-phase polymerization

Different UHMWPE samples were synthesized in slurry and gas phase, using a commercial Ziegler-Natta catalyst. Polymerizations were performed over a range of temperatures and ethylene pressures. In addition, different alkanes were used as an induced condensing agent (ICA). Pertinent polymerization data are collected in **Table 1**. No reactor

fouling was observed in any of the polymerizations, and the product was always a free-flowing powder. Representative results of powder morphology are shown in **Figure 1**. The powder from gas phase experiments was generally finer, with fewer agglomerates. When agglomerates are present in the gas phase they appear to be formed from well-defined particles of a size very similar to that of the other particles. Agglomerates seem to be formed more frequently in the slurry processes and appear to be somewhat less well-defined than in the gas phase. It is difficult to say whether the aggregates in either of the processes are formed during the emptying and drying processes, or during the polymerization phase. It is even possible that static charges on the small catalyst particles cause the aggregates to form even before they are injected into the reactor. While particle morphology is an important issue in a commercial process, it is a complex issue that outside of the scope of the current paper.

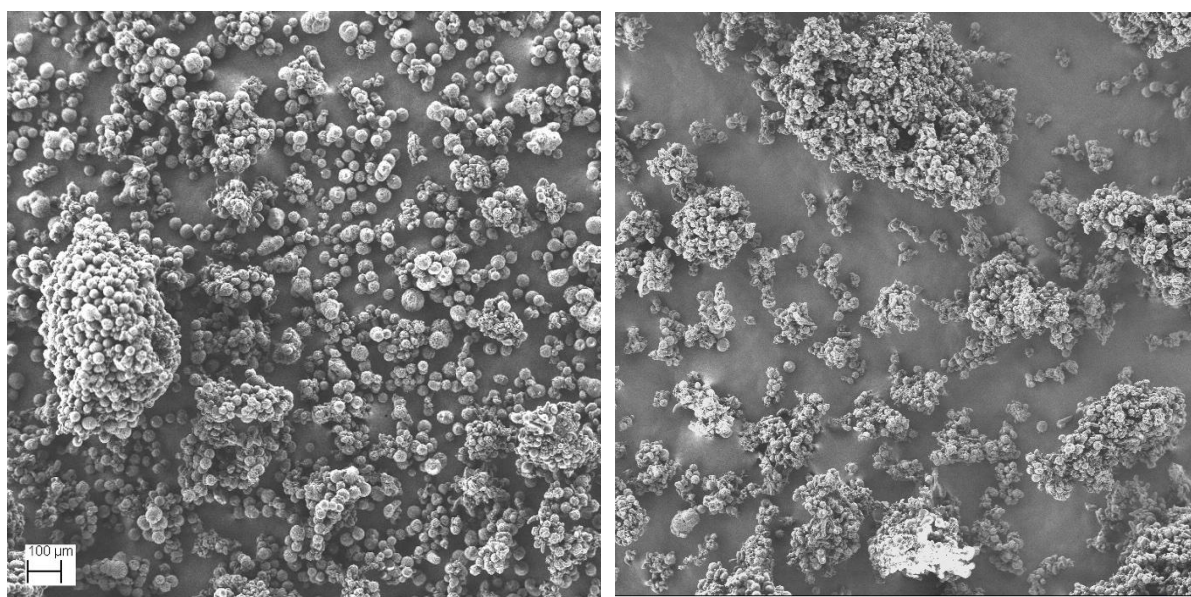


Figure 1: Reactor powder morphology from samples made in a gas phase process (left) and in a slurry phase process (right). Both images are at the same scale. The polymerizations were performed at 70°C. The gas phase polymerization was with 4 bar of ethylene and 0.4 bar of hexane. The slurry polymerization was performed in hexane with 6 bar of ethylene.

The experiment names indicate the pertinent conditions: in the experiment V-XX-YZ_w, V refers to the phase (S for slurry, G for gas), XX to the polymerization temperature in °C, Y to the ethylene pressure, Z to the alkane used in the experiment (D for decane, H for hexane and P for pentane), and if there is subscript _w it indicates different partial pressures of alkane in the gas phase experiments in case a value different from 0.4 bar is used. As an example, G-50-4P_{0.4} refers to a gas-phase polymerization at 50 °C and 4 bar ethylene pressure, using Pentane with a pressure of 0.4 bar as ICA.

The melting temperatures and crystallinities displayed no strong dependence on the polymerization conditions and were found to be around 140-143 °C and 60-65%, respectively. Hexane and decane were chosen for the comparative slurry polymerizations to evaluate the eventual impact of any differences in swelling by alkanes of different molecular weights. As decane is not volatile at gas phase reaction conditions, the comparison is made with n-hexane and n-pentane in the gas phase experiments.

Table 1. Abbreviated names, polymerization conditions, like mode, temperature, ethylene pressure and concentration, ICA and ICA pressure, and viscosity average molecular weight, crystallinity (x_{DSC}), melting point ($T_{m,DSC}$), (M_v) and maximum draw-ratio (λ_{max}) of the UHMWPE grades used.

Nr	Abbr. Name	Polymerization Mode	T [°C]	$P_{ethylene}$ [bar]	$C_{ethylene}$ [mol L ⁻¹]	Alkane	P_{alkane} [bar]	M_v [kg mol ⁻¹]	x_{DSC} [%]	$T_{m,DSC}$ [°C]	λ_{max} [-]
1	S-70-6D	Slurry	70	8	0.51	Decane	-	5500	62.1	142.7	7 +/- 1
2	S-70-6H	Slurry	70	6	0.51	Hexane	-	5000	62.8	142.4	11 +/- 2
3	S-60-6H	Slurry	60	6	0.57	Hexane	-	5150	60.0	142.6	9 +/- 2
4	S-50-4H	Slurry	50	4	0.40	Hexane	-	7000	57.1	142.7	10 +/- 3
5	G-70-15H	Gas	70	15	0.51	Hexane	0.4	4700	64.8	142.7	21 +/- 2
6	G-70-4H	Gas	70	4	0.15	Hexane	0.4	2000	64.4	140.0	28 +/-3
7	G-60-15H	Gas	60	15	0.57	Hexane	0.4	3700	61.3	143.3	19 +/- 4
8	G-50-10H	Gas	50	10	0.40	Hexane	0.4	5300	62.6	143.1	33 +/- 2
9	G-50-4H	Gas	50	4	0.15	Hexane	0.4	5500	62.0	143.0	41 +/- 4
10	G-50-3H	Gas	50	3	0.11	Hexane	0.4	5100	62.0	142.7	51 +/-5
11	G-70-15P	Gas	70	15	0.51	Pentane	0.4	3700	63.3	142.2	28 +/-3
12	G-70-4P	Gas	70	4	0.15	Pentane	0.4	2000	64.2	143.0	48 +/-6
13	G-50-4P _{0.4}	Gas	50	4	0.15	Pentane	0.4	5350	66.0	141.1	88 +/- 4
14	G-50-4P _{1.3}	Gas	50	4	0.15	Pentane	1.3	5450	66.1	142.0	86 +/- 5
15	G-40-4P	Gas	40	4	0.15	Pentane	0.4	6200	64.3	141.1	97 +/- 5
16	G-50-4	Gas	50	4	0.15	-	-	3100	65.0	142.2	43 +/- 6
17	G-70-15	Gas	70	15	0.51	-	-	1900	63.0	142.6	12 +/-0

3. Evaluation of the entanglement density

Disentangled reactor powders, compacted below the melting temperature, can be drawn to high draw ratios in the solid state.^[17,18] The maximum achievable draw-ratio (λ_{\max}) scales with the amount of entanglements according to Equation 1, where M_e corresponds to the molecular weight between entanglements, N_e is the number of segments between entanglements, L_0 is the monomer length and c_∞ is the characteristic ratio:

$$\lambda_{\max} = \frac{N_e L_0}{\sqrt{c_\infty N_e L_0^2}} \sim \sqrt{N_e} \sim \sqrt{M_e} \quad (1)$$

UHMWPE reactor powders were evaluated in terms of maximum draw ratio polymerized both via slurry- and gas-processes and the measured λ_{\max} values are reported in Table 1. Several comparisons are presented in **Figure 2**, to elucidate the effect that different polymerization conditions, like slurry or gas-phase polymerization, polymerization temperature (T_{pol}), alkane choice as ICA and ethylene pressure (P_{ethylene}), have on the level of entanglement of the polymerized powder.

First, it can be seen from Figure 2A that when the rest of the polymerization conditions are kept the same, the change from slurry to gas-phase polymerization results in an increase in λ_{\max} of tapes prepared by each UHMWPE powder, indicating that the samples produced through gas-phase polymerization are noticeably more disentangled, regardless of the type of alkane in each type of experiment. For this, samples S-70-6H to G-70-15H, S-60-6H to G-60-15H and S-50-4H to G-50-10H were compared respectively. The ethylene pressure differs in the slurry and gas-phase polymerization pairs performed at the same temperature with the aim to keep the ethylene concentration in the continuous phase the same (i.e. the same number of mol L⁻¹ in the diluent for slurry and in the gas for gas phase). The reason for this is to isolate the effect of the alkane at equivalent ethylene concentrations outside the particles.

Next, the effect of the alkanes themselves on the resulting entanglement density was investigated. Two samples polymerized in slurry at the same temperature and ethylene pressure, but in the presence of decane and hexane respectively, were compared (S-70-6D and S-70-6H). A slight increase in λ_{\max} is observed in the sample with hexane. The rest of the samples shown in Figure 2B are prepared through gas-phase polymerization and are samples prepared with hexane or pentane as ICA. The sample pairs with different ICAs are G-70-15H to G-70-15P, G-70-4H to G-70-4P and G-50-4H to G-50-4P_{0.4}. Using a lighter alkane leads to an increase in λ_{\max} . This could be due to different rates of polymerization and/or crystallization in the presence of different alkanes, and will be investigated in the following section. The effect of polymerization temperature on λ_{\max} showed that, a decrease in temperature results in higher values of λ_{\max} (Figure 2C). A decrease in temperature will decrease the catalyst activity, lowering the polymerization rate, while at the same time decreasing temperatures will increase the undercooling, which increases the crystallization rates. Both of these effects are expected to reduce the entanglement density of the produced polymer, as the rate by which the macromolecular chains are formed is decreased, while the rate at which they crystallize is higher, thus leaving less time for the chains to form intermolecular entanglements. For this comparison, gas-phase polymerized, samples with hexane (G-70-4H, G-50-4H) and pentane (G-70-4P, G-50-4P_{0.4}, G-40-4P) as ICA were used. In addition, samples polymerized with a different ethylene pressure, while keeping the rest of the polymerization conditions same, were evaluated. A lower ethylene pressure, is known to reduce the entanglement density in UHMWPE reactor powder prepared through a slurry process.^[18] A similar trend was observed for gas-phase polymerized samples presented in Figure 2D, where a decrease in the ethylene pressure is resulting to increase in λ_{\max} , with the effect being more significant for samples polymerized at a lower temperature. The samples that were compared towards that end were G-70-4H to G-70-15H, G-70-4P to G-70-15P and G-50-3H to G-50-10H. Last, two samples (G-50-4P_{0.4} and G-50-4P_{1.3}) prepared in the gas-

phase with a different ICA pressure were compared, however no considerable different in λ_{\max} was found.

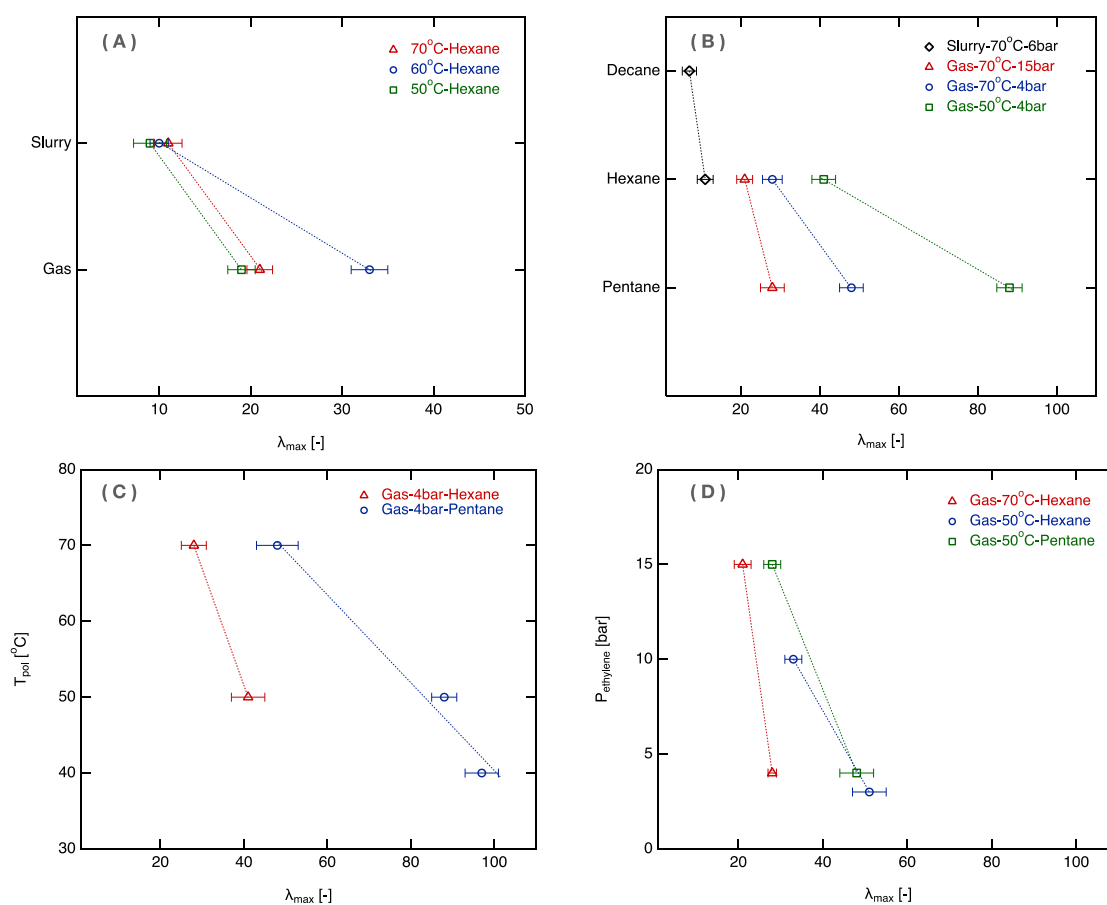


Figure 2. Comparison of the maximum achieved draw-ratio for UHMWPE samples produced under different polymerization conditions. (A) Effect of polymerization mode. Red triangles: samples 2 and 5; blue circles: samples 3 and 7; green squares: samples 4 and 8. (B) Effect of different ICAs. Black diamonds: samples 1 and 2; red triangles: samples 5 and 11; blue circles: samples 6 and 12; green squares: samples 9 and 13. (C) Effect of polymerization temperature. Red triangles: samples 6 and 9; blue circles: samples 12, 13 and 15. (D) Effect of ethylene pressure. Red triangles: samples 6 and 7; blue circles: samples 8 and 10; green squares: samples 11 and 12. The dashed lines are a guide to the eye.

4. Crystallization kinetics

The crystallization kinetics were examined to understand how they are impacted by the conditions in which the chains crystallize (gas, slurry, type of alkane) during polymerization. To do so, calorimetric experiments were run at different cooling rates using dry (i.e. no liquid) UHMWPE samples and samples with a small excess liquid that vaporizes during the experiments to simulate crystallization in the gas phase (10 μL of ICA at room T) or with enough ICA that it remains liquid ICA (40 μL) in the DSC capsules to simulate crystallization under slurry conditions.

It is important to note that these experiments do not really replicate the condition of crystallization in the reactor, as during the DSC experiments, the macromolecular chains crystallize from the isotropic melt, in contrast to as-polymerized polyethylene chains during gas-phase polymerization. In addition, the effect of the polymerization rate is not considered. For the analysis, the isoconversional method was employed and apparent activation energy values for different degrees of conversion were calculated for each sample. The dependence of apparent activation energy on conversion is changed to be dependent on temperature as to enable its parameterization according to the Hoffman-Lauritzen theory for polymer crystallization.^[23–25] The temperature variation of the apparent activation energy is then related to the intrinsic energy barriers (U^* and K_g) of the Hoffman-Lauritzen theory:^[23–26] The temperature variation of the apparent activation energy is then linked to the intrinsic energy barriers (U^* and K_g) of the Hoffman-Lauritzen theory:^[25]

$$E_\alpha = U^* \frac{T^2}{(T-T_\infty)^2} + K_g R \frac{T_m^{0^2} - T^2 - T_m^0 T}{(T_m^0 - T)^2 T} \quad (2)$$

Where U^* is the activation energy of the segmental jump, T is the temperature, T_∞ is the temperature at which viscous flow ceases, defined as $T_g - 30\text{K}$, T_m^0 is the equilibrium melting temperature, R is the universal gas constant and K_g is a constant related to the nucleation process i.e. rate of formation of crystal nuclei. The temperature is used to introduce

non-Arrhenius-like behavior as the crystallization temperature approaches T_g , which in the case of polyethylene that has a very low T_g compared to the crystallization temperature can be omitted, reducing Equation 2 to:

$$E_\alpha = Q_d^* + K_g R \frac{T_m^0 - 2T}{(T_m^0 - T)^2} \quad (3)$$

where Q_d^* is the activation energy of the reptation process, taken as 24 kJ mol⁻¹ and assumed to be independent of the presence of ICA.^[26,27] Equation 3 is fitted to the E_α against T curves obtained from the isoconversional analysis with K_g and T_m^0 as fitting parameters. The different experimental conditions are evaluated in terms of K_g and undercooling (ΔT), where a higher value in both these parameters would correspond to a faster crystallization. The undercooling is calculated from the estimated T_m^0 and the crystallization temperature obtained at a cooling rate of 10 °C min⁻¹. The calculated crystallization parameters are presented in **Table 2** for measurements made using sample G-50-4P_{0.4} and using an entangled sample of commercial UHMWPE obtained from SABIC.

Table 2. Crystallization parameters of the crystallization experiments of UHMWPE with different amounts of different alkanes as induced condensing agents in order to imitate crystallization at different polymerization conditions.

Sample	ICA [μL]	K_g [K ²]	T_m [K]	ΔT [K]	K_g [K ²]	T_m [K]	ΔT [K]
		G-50-4P _{0.4}			Entangled Commercial Sample		
Slurry Decane	40	8.6 x 10 ³	376.8	15.9			
Slurry Hexane	40	5.8 x 10 ³	374.3	10.6	1x10 ⁴	371	12.8
Slurry Pentane	40	2.5 x 10 ³	374.1	12.8			
Gas-phase Decane	10	2.5 x 10 ⁴	384.9	17.6			
Gas-phase Hexane	10	2.1 x 10 ⁴	382.8	17.2	6.5x10 ⁵	383	21.6 K
Gas-phase no ICA	-	1.2 x 10 ⁵	414.5	21.4			

^{a)}Gas-phase experiments with pentane as ICA are not included due to evaporation of the pentane during the sample preparation.

The lowest values for both ΔT and K_g , indicating the lowest crystallization rate, are found for the slurry-imitating experiments, where 40 μL of alkane is added. A slow crystallization would give more time to the as-polymerized chains to form entanglements, which agrees with the findings of the solid-state drawability experiments, where the lowest measured values of λ_{max} are found for materials prepared through slurry polymerization. In contrast, the fastest crystallization is identified for the sample where no alkane is added, that represents the gas-phase polymerization with no addition of ICA, however as mentioned earlier, the molecular weight of samples prepared in that way is quite low and cannot be classified as UHMWPE.

For the experiments that mimic the environment of gas-phase polymerization in the presence of ICA, the crystallization rate is found to be lower compared to the gas-phase with no ICA, but still faster than in the slurry-like experiments, showing that these polymerization conditions produce polyethylene with a good compromise between low entanglement density and high molecular weight, in agreement with the findings from Figure 2A. Furthermore, a relatively small difference in both ΔT and K_g is found for the different alkanes when they are used in the same concentrations. Furthermore, the value of K_g seems to decrease slightly the lighter the alkane becomes. Although a limited number of experiments were done with the commercial sample, the crystallization parameters calculated for that grade agree with the ones calculated for the sample G-50-4P_{0.4} and show the same trend of faster crystallization in the gas-phase imitating experiment compared to the slurry one, showing that this observation is not UHMWPE grade dependent.

5. Microstructure analysis

The microstructure of the reactor powder was examined in terms of lamellar thickness through small-angle X-ray scattering (SAXS) experiments. The lamellar thickness of several UHMWPE reactor powders was estimated and correlated to the λ_{\max} of ultra-drawn tapes prepared from the same material as shown in **Figure 3**. It can be observed that the thinner the lamella the higher the value of λ_{\max} , in agreement with literature.^[28] This can be explained through the standard theory of polymer crystallization, where it is stated that fast crystallization leads to polymer crystals with a thinner lamella.^[29] It was shown earlier that during gas-phase polymerization, where the reaction results in more disentangled samples, the crystallization rate is faster compared to polymerization in slurry. Similarly, a small increase was observed by using a lighter alkane and naturally the decrease in polymerization temperature results into a higher undercooling, known to lead to polymer crystals with a thinner lamella. The faster crystallization, evident by the thinner lamella, reduces the chance of the formation of entanglements of the growing macromolecular chain, which in turn is depicted in the larger values of λ_{\max} .^[17,28]

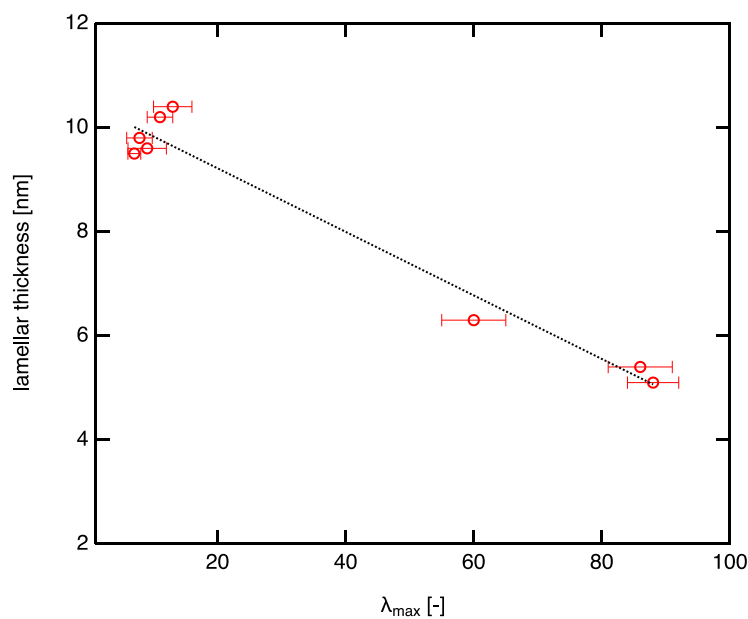


Figure 3. Lamellar thickness against maximum draw ratio (λ_{\max}) for different UHMWPE samples. The dashed line is a guide to the eye.

6. Fiber properties

From an application and industrial perspective two aspects are important. First, the control over powder morphology, that is being achieved through the Ziegler-Natta catalyst used in the present study. Second the properties of UHMWPE fibers manufactured from the as-polymerized powder, as this area is currently the biggest market for disentangled UHMWPE, with an important aspect being the tenacity of these fibers. For that reason, fiber samples were created through ultra-drawing of calendered tapes made from the most promising (highest λ_{\max}) UHMWPE powders and evaluated in terms of tenacity. The measured values of tenacity against draw-ratio are presented in **Figure 4**, together with comparative data from literature. The highest values for tenacity, up to almost 4 N/tex, are reported in the work of Rastogi et al., using a single-site, homogeneous, catalytic system.^[30] However, as already mentioned, this results in severe reactor fouling and would be difficult to implement on an industrial level. The rest of the comparative data included in Figure 4 are samples polymerized with heterogeneous low-activity Ziegler-Natta catalysts in slurry and under mild polymerization conditions from the same work of Rastogi et al.^[30], the work of Kanamoto et al.^[31] and from a patent by DSM.^[32] The samples made by Ziegler-Natta catalysts constitute materials with a similar entanglement density as what is currently the industrial standard for solid-state processed high strength and high modulus UHMWPE tapes. The tenacity of the tapes produced in the present work, from gas-phase polymerized UHMWPE, is on par with the industrial standard, showing that this could be a viable processing route for technologically relevant applications.

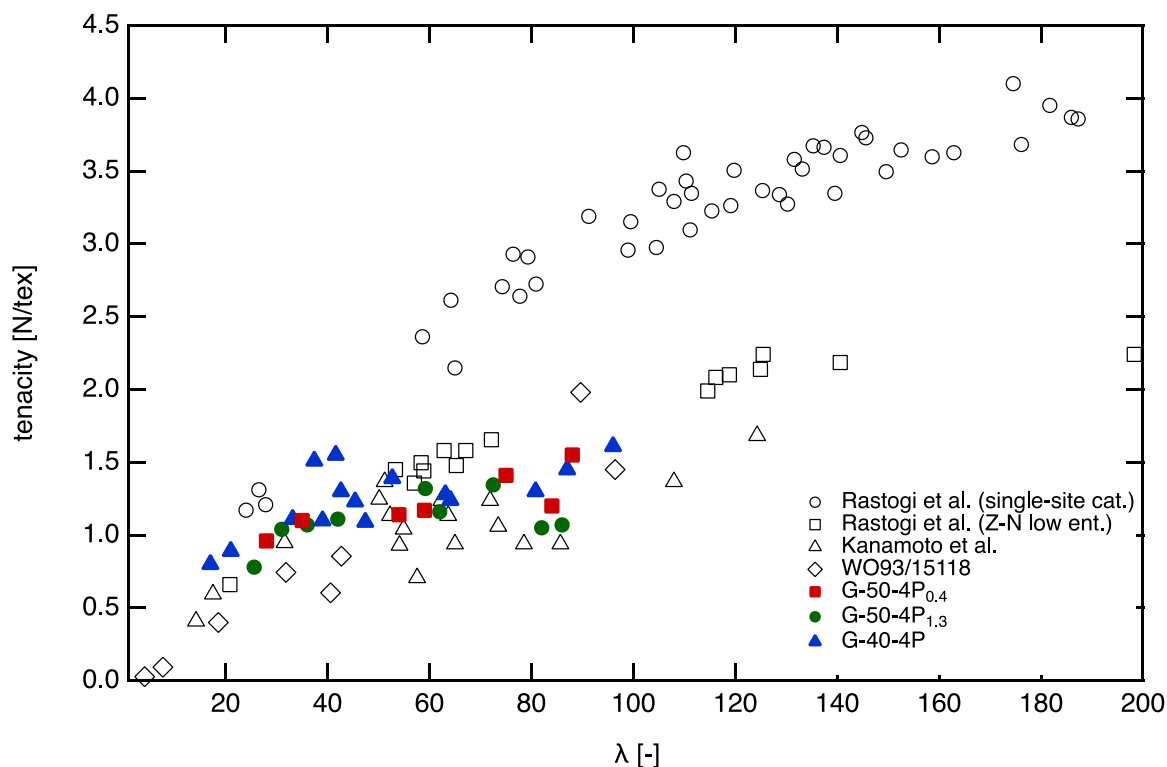


Figure 4. Comparative data of UHMWPE fiber properties against draw-ratio found in literature (Rastogi et al.^[30], Kanamoto et al.^[31], WO93/15118^[32]) plotted along with the results from fibers made by UHMWPE polymerized in the gas-phase (G-50-4P_{0.4}, G-50-4P_{1.3}, G-40-4P).

7. Conclusion

The standard way for the production of high-performance UHMWPE fibers is the gel-spinning route. However, an alternative method, which avoids the use of excessive amounts of solvent, is solid-state processing of low-entangled UHMWPE reactor powder. Similar to gel-spinning, the lower the entanglement density of the reactor powder, the higher is the maximum achievable draw ratio, leading to superior fiber properties. Currently, disentangled UHMWPE powder can be produced through homogeneous, single-site, unsupported catalysts, which however result in severe reactor fouling, making them unsuitable for industrial applicability. Industrially, low-entangled UHMWPE reactor powder made through Ziegler-Natta catalysts in slurry and at mild polymerization conditions are used for the solid-state processing of UHMWPE into high-performance fibers and tapes. In our work, we

demonstrate the feasibility of producing low-entangled UHMWPE through a Ziegler-Natta catalyst when the polymerization is carried out in the gas-phase, while retaining control over powder morphology. The same catalyst, when used for the production of UHMWPE in slurry, yields a highly entangled sample, that cannot be converted to high-performance UHMWPE fibers. By analyzing the crystallization kinetics through DSC experiments, it was found that in gas-phase polymerization, the newly formed macromolecular chains crystallize faster compared to polymerization in slurry. A faster crystallization hinders the formation of intermolecular entanglements. As expected, and in agreement with literature, a decrease in polymerization temperature or ethylene pressure resulted to a decrease in the entanglement density of the reactor powder. It was also observed that the lighter the alkane, used as induced condensing agents, the more disentangled is the produced reactor powder. The effect of the different ICAs could be looked into more systematically and by introducing even lighter alkanes like butane in the study. The present work establishes the possibility to produce low-entangled UHMWPE by gas-phase polymerization. The polymerization conditions could be further optimized and moreover different catalytic systems could be tried out. UHMWPE fibers processed from gas-phase produced reactor powder have tenacity values on par with commercial materials.

8. Experimental Section

Polymerization Materials: Ethylene with a minimum purity of 99.5% obtained from Air Liquide (Paris, France) was passed over purifying columns of zeolite and active carbon before use. Argon with a minimum purity of 99.5%, used to keep the reaction environment free of oxygen and other impurities, was obtained from Air Liquide. Triisobutylaluminium (TiBA) co-catalyst was obtained from Witco (Germany). A commercial TiCl_4 supported on MgCl_2 Ziegler-Natta catalyst provided by SABIC with a particle size of around $4.5 \mu\text{m}$ with a Ti content of 5.5 wt% was used as the catalytic system for all polymerizations.^[33] The heating of the reactor is achieved through a water jacket connected to a heat exchanger, whereas the cooling is done using cooling water at ambient temperature.

The polymerization experiments were performed in a spherical stirred-bed semi-batch reactor shown in the diagram in **Figure 5**.

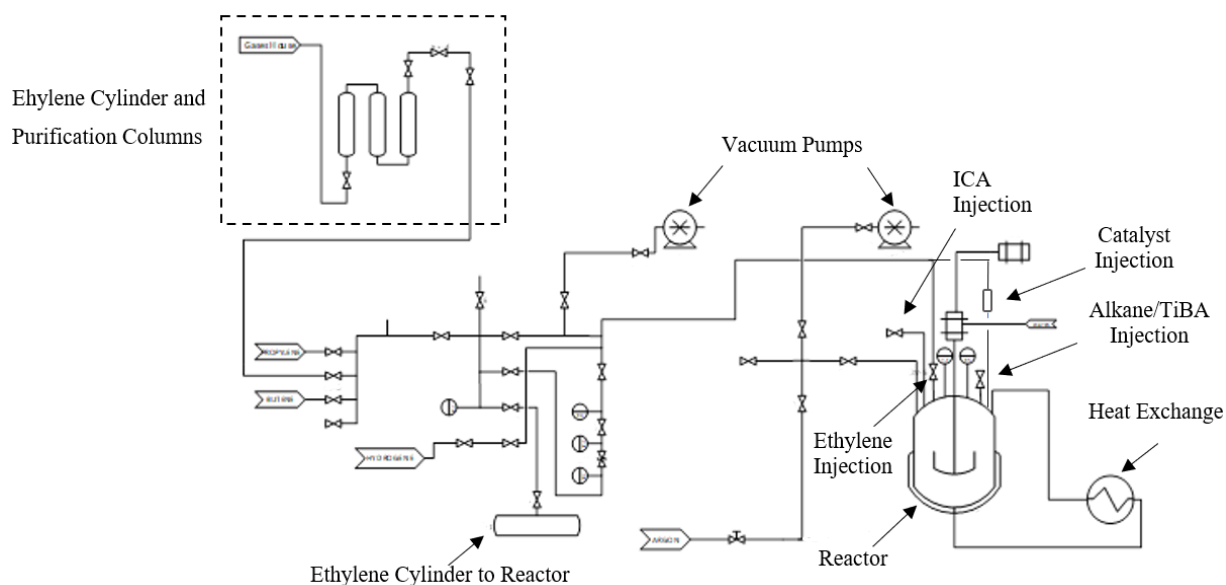


Figure 5. Schematic representation of the experimental setup used for the slurry and gas-phase polymerization.

Polymerization in slurry: N-hexane (minimum purity 99.3%, from AnalaR Normapur) or n-decane (minimum purity 99%, from abcr) were used as diluents in the slurry reaction. The diluent was purified by bubbling the solvent, containing a molecular sieve with a pore

size of about 4 Angstrom from Fisher Scientific, with argon for 2 hours. After that, the mixture was kept on the molecular sieves for five to six hours.

Gas-phase Polymerization: Sodium chloride (NaCl) with a minimum purity of 99.8% from Carl RothTM was used as a seedbed to disperse the catalyst particles. The salt was dried under vacuum for two hours at 200 °C and an additional 4 hours at 400 °C before use, to eliminate all traces of water. The alkanes used as an Induced Condensing Agent (ICA), n-hexane (minimum purity 99,3%, from AnalaR Normapur) and n-pentane (minimum purity 99%, from Sigma-Aldrich ICN - Germany), were purified 3-4 Angstroms and stored in Schlenk flasks containing molecular sieves. The ethylene solubility in decane was measured using a pressure decay experiment as described in reference [34],^[34] and the ethylene solubility in hexane was found in reference [35].^[35]

Polymerization Reaction: The reactor was first heated to 80 °C under vacuum for at least 1 hour to remove any trace of moisture. Subsequently, it was cooled down to room temperature before the injection of the reagents. In the slurry polymerizations, a cannula was used to transfer 500 mL of alkane from a Schlenk tube to the reactor and a syringe used to inject a solution of triisobutylaluminium (TiBA). Once closed, the agitation in the reactor was adjusted to 500 rpm, the mixture was heated up to the desired temperature and the catalyst was injected using ethylene over-pressure from the ballast. The reaction started setting up the ethylene pressure from the ballast to the reactor. The reaction temperature, ethylene pressure in the ballast and the reaction time were monitored. In gas phase polymerizations, salt was transferred from a Schlenk tube directly to the reactor and TiBA was injected using a syringe. The reactor was closed, the agitation was adjusted to 300 rpm and heated up to the reaction temperature. Subsequently, the alkane was injected using an injection pump until the required

pressure was achieved. Similar to the reaction in slurry, the catalyst was then injected, and the reaction started.

For slurry and gas phase, 1 M TiBA was diluted in the respective alkane, present in the reaction. On the other hand, for the reaction with no presence of ICA, TiBA was not diluted in alkane. The procedure was designed to avoid the pre-contacting of the catalyst, where directly after the injection of the catalyst into the reactor, the alkyl aluminum, present in the reactor, activates the catalyst under polymerization conditions. The reactions were carried out using Al/Ti ratio of 170 for all conditions.

Thermal analysis: For the thermal analysis, DSC experiments were conducted with a Mettler Toledo DSC3+, calibrated with Indium and Zinc standards for temperature, heat flow and tau-lag. For the experiments with pure UHMWPE powder, aluminium capsules with a volume of 40 μL and a sample weight of 2 mg ($\pm 50 \mu\text{g}$). were used. For the evaluation of the crystallization kinetics UHMWPE powder was loaded together different amounts of ICA into medium-pressure pans with a volume of 120 μL . DSC thermographs were recorded under N_2 flow of 20 L min^{-1} and a value of 293 J g^{-1} was used for the heat of fusion of polyethylene.^[36] For each experiment a new sample was used.

Viscosity average molecular weight: In order to estimate the viscosity average molecular weight (M_v) of the polyethylene samples, the intrinsic viscosity (IV) was measured with a Polymer Char Intrinsic Viscosity Analyser (IVA). Vials with pre-weighted amount of polymer were placed into the external tray of the autosampler, at room temperature. Next, the vials are placed into the dissolution oven, filled with 16 mL of trichlorobenzene (TCB) shaken under nitrogen atmosphere at 150 $^\circ\text{C}$ for 3 hours. The M_v was calculated from IV data, provided by the measuring instrument, following the Mark-Houwink equation.^[37] Since the equipment used for the IV measurements is a prototype, a calibration step for evaluating

UHMWPE was necessary. Therefore, different amounts of polymer were dissolved in 16 mL of TBC. Polyethylene grades with known IV values were used for the calibration and the best agreement was found when 2 mg of polymer are dissolved in 16 mL of TBC.

Morphology: Scanning Electron Microscopy (SEM) was accomplished with the samples synthesized at the “Centre Technologique des Microstructures” (CTμ) using an MEB ZEISS Merlin Compact microscope under a high vacuum and with accelerating voltages of 5 to 10 keV. The powder samples were fixed on a standard aluminum slotted head covered with carbon adhesive and coated with 10 nm of Cu.

Solid-state drawability: For the preparation of the solid-state drawability specimen, 200 g of UHMWPE reactor powder were compression molded at 200 bar and 120 °C, below the melting temperature, for 20 min into 1 mm thick films. The films were then drawn in the solid-state in a two-step process. First, to a draw ratio (λ) of about 4 by calendering, using a Scamex MC100LABO 400V calendering machine, at 125 °C. Subsequently, dumbbell-shaped samples, according to ISO 527-2 type 5B, were cut from the calendered films and drawn in an Instron 5864 static mechanical tester, equipped with an environmental-control chamber, at 130 °C at an initial strain rate of 0.1 s⁻¹, until failure occurred. The draw-ratio is calculated from the displacement of the cross-head and is the mean value of at least five measurements. The maximum draw ratio (λ_{max}) of each sample corresponds to the product of the two drawing steps.

Isoconversional analysis: Isoconversional analysis evaluates reactions at the same extent of conversion, α , from data acquired through calorimetric experiments with different temperature programs. This is achieved in a model-free way, without assuming a reaction model beforehand.^[24,38-41] In the case of crystallization of polymers this can be achieved by

conducting non-isothermal, constant cooling rate experiments with a different cooling program (cooling rate, β) between each experiment. Isoconversional kinetic analysis evaluates a dependence of the apparent activation energy, E_α , on conversion or temperature of thermally stimulated processes.^[24,39] The general form of the basic rate equation for thermally stimulated processes can be written as:

$$\frac{d\alpha}{dt} = k(T, \alpha)f(\alpha) \quad (4)$$

where α is the extent of crystallization (“conversion”), which takes values from 0 (fully molten) to 1 (fully crystallized), t is the time, T is the temperature, $f(\alpha)$ is the mathematical function that represents the reaction model, and $k(T)$ is the rate coefficient.^[42] The dependence of the rate coefficient on temperature is typically given by an Arrhenius law:^[43] where α is the extent of crystallization (“conversion”), which takes values from 0 (fully molten) to 1 (fully crystallized), t is the time, T is the temperature, $f(\alpha)$ is the mathematical function that represents the reaction model, and $k(T)$ is the rate coefficient.^[42] The dependence of the rate coefficient on temperature is typically given by an Arrhenius law:^[43]

$$k(T, \alpha) = A(\alpha)e^{-E(\alpha)/RT} \quad (5)$$

where A is a pre-exponential factor, E is the activation energy and R is the universal gas constant. The isoconversional principle states, that at a constant extent of conversion, the reaction rate is only a function of temperature and so according to Equation 4:^[44]

$$\left[\frac{\partial \ln(d\alpha/dt)}{\partial T^{-1}} \right]_\alpha = \left[\frac{\partial \ln k}{\partial T^{-1}} \right]_\alpha + \left[\frac{\partial \ln f(\alpha)}{\partial T^{-1}} \right]_\alpha \quad (6)$$

The subscript α indicates values related to a certain extent of conversion and since $f(\alpha)$ does not depend on temperature when α is constant:

$$\left[\frac{\partial \ln(d\alpha/dt)}{\partial T^{-1}} \right]_\alpha = -\frac{E_\alpha}{R} \quad (7)$$

In that way a model-free value of the apparent activation energy can be estimated. For that, an integral or a differential method can be employed. Since the data is already in a differential form as it originates from DSC measurements, the differential isoconversional method of

Friedman was used.^[39] For this method the knowledge of several triplets of reaction rate, temperature and conversion are required. For this method the knowledge of several triplets of reaction rate, temperature and conversion are required. By combining Equation 4 and 5 we get:

$$d\alpha/dt = A(\alpha)f(\alpha)e^{-E(\alpha)/RT} \quad (8)$$

and by using the isoconversional method at a constant extent of conversion, α :

$$\ln\left(\frac{d\alpha}{dt}\right)_{\alpha,i} = \ln[f(\alpha)A_{\alpha}] - \frac{E_{\alpha}}{RT_{\alpha,i}} \quad (9)$$

where $\ln[A_{\alpha}f(\alpha)]$ is constant. The apparent activation energy E_{α} can be determined by plotting the left-hand side of Equation 9 and calculating the slope of the resulting Arrhenius-like plots.

Small- and wide-angle X-ray scattering: Simultaneous small- and wide-angle X-ray scattering experiments were performed at the BM02 beamline of the European Synchrotron Radiation Facilities (ESRF, Grenoble, France). An energy of 17.5 keV was used with a sample-detector distance of 175 cm and 17 cm for the small- and the wide-angle measurements, respectively. The samples measured consisted of as-polymerized powder and the measurements were conducted at room temperature. The powder sample was fixed in the middle of an aluminum ring with a polyimide (Kapton) film on both sides to hold the polymer in the ring.

Before evaluating the data, the scattering curves were calibrated (q-axis) using silver behenate and corrected for sample transmission and background subtraction. Glassy carbon was used for the absolute intensity scaling. The scattered intensity was recorded as a function of the scattering vector q , defined as $q = 4\pi/\lambda \sin(\theta)$, where 2θ is the angle between the incident beam and the detector, measuring the scattering intensity, and λ is the wavelength of the radiation. The Lorentz-correction was applied to the recorded curves. The average long period L of the lamellar stacking, was determined from the q -value, q_{\max} , at which the Lorentz-

corrected intensity reached a maximum, using the Bragg's condition: $L = 2\pi/q_{\max}$. Since the scattering features is identifiable only at ultra-small angles, in order to identify the matching point more precisely, the generalized Porod power law was added ^[26,45]:

$$I(q \gg q_0) \rightarrow \frac{A_1}{q^{6-D_1+I_0}} \quad (10)$$

Where D_1 is the surface fractal dimension of the crystalline-amorphous interface, and A_1 is proportional to the surface-to-volume ratio, I_0 is the scattering intensity. These data were plotted and analyzed in the graphs showed in Figure 6.

The lamellar thickness l was calculated by multiplying the long period with the crystal volume fraction measured through WAXS. ^[46]

SAXS measurements were analyzed using the SASfit 0.93.3 software. The crystallinity was evaluated from the ratio of the crystalline peaks of 110 and 200 spacing to the total intensity of the crystalline and the amorphous parts obtained through the WAXS measurements. The internal comparison method of Ruland was followed and the correction factor for polyethylene from Mo et al. were used. ^[47,48]

Fiber properties: The mechanical properties were measured on fibers prepared through ultra-drawing of dumbbell-shaped specimen punched out from calendered UHMWPE films, with a calendering draw ratio of 3. For the measurement an Instron 5864 static mechanical tester was used at room temperature and with an initial cross-head speed of 0.1 s^{-1} .

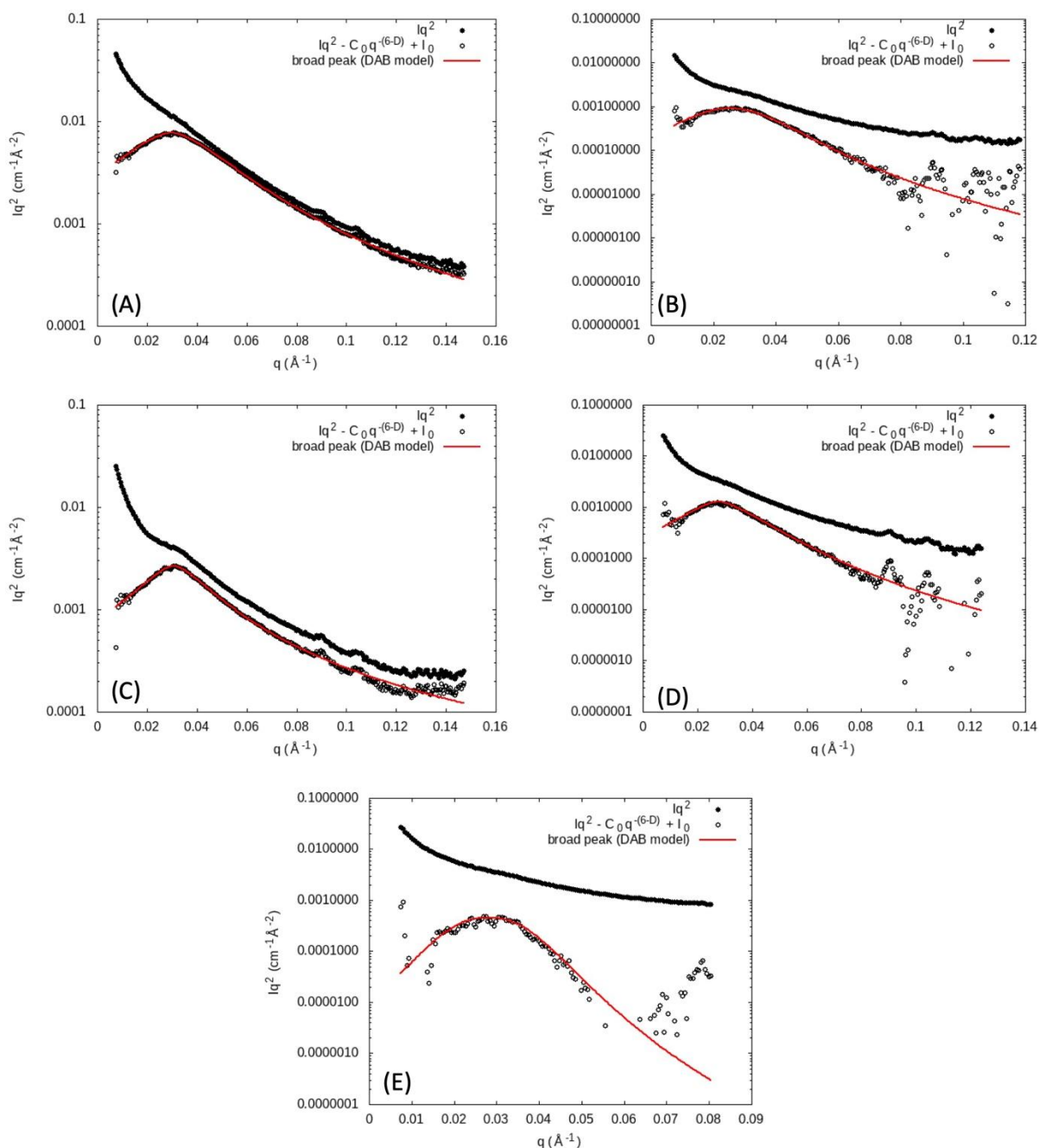


Figure 6: Plotting of SAXS data of (●)Lorentz-corrected scattering intensity (Iq^2), (○) Iq^2 after subtraction of background function, (—)Fitting of the peak to provide q_0 value, from the samples (A) S-70-9D, (B) G-70-15P_{0.4}, (C)G-70-4P_{0.4}, (D) G-70-15, (E) G-60-15H_{0.4}

Acknowledgements

This research forms part of the research programme of DPI, project #814t18. The authors thank Dr. Nic. Friederichs and Dr. Enrico Troisi from SABIC T&I Geleen for

providing the catalyst used in the study, help with the preparation of the fibers and fruitful discussions. F.C. gratefully acknowledges funding by SABIC. The authors also thank Isabelle Morfin for her help on the ESRF: BM02 - D2AM French CRG Beamline.

Conflict of Interest

The authors declare no conflicts of interest.

Received: ((will be filled in by the editorial staff))
Revised: ((will be filled in by the editorial staff))
Published online: ((will be filled in by the editorial staff))

References

1. INTERNATIONAL STANDARD ISO 21304-1 Plastics — Ultra-high-molecular-weight polyethylene (PE-UHMW) moulding and extrusion materials, 2019, vol. 21304– 1:20.
2. Ultra-High-Molecular-Weight Polyethylene Molding and Extrusion Materials - ASTM D4020-11, 2005.
3. Celanese, ultra-high molecular weight polyethylene, <https://www.celanese.com/products/gur-uhmw-pe-ultra-high-molecular-weight-polyethylene> accessed: November 2022.4. Kurtz, S. M. The UHMWPE Handbook, Academic Press, San Diego, 2004.
5. Ciferri, A., Ward, I. M. Ultra-high Modulus Polymers, Applied Science Publishers, 1979.
6. Balzano, L., Coussens, B., Engels, T., Oosterlinck, F., Vlasblom, M., Van Der Werff, H., Lellinger, D. *Macromolecules*, 2019, **52**, 5207–5216.
7. Rao, Y., Waddon, A. J., Farris, R. J. *Polymer (Guildf)*., 2001, **42**, 5937–5946.
8. Herrbach, P. High-performance fibres, CRC Press Woodhead Pub, Cambridge, England, 2001.
9. Smith, P., Lemstra, P. J. *J. Mater. Sci.*, 1980, **15**, 505–514.
10. Smith, Paul; Lemstra, Piet, J; Booij, Henk, C. *J. Polym. Sci.*, 1981, **19**, 877–888.
11. Smith, P., Lemstra, P. J. *Polymer (Guildf)*., 1980, **21**, 1341–1343.
12. Schaller, R., Feldman, K., Smith, P., Tervoort, T. A. *Macromolecules*, 2015, **48**, 8877–8884.
13. Antonov, A. A., Bryliakov, K. P. *Eur. Polym. J.*, 2021, **142**, 110162.
14. Romano, D., Andablo-Reyes, E., Ronca, S., Rastogi, S. *Polymer (Guildf)*., 2015, **74**, 76–85.
15. Ronca, S., Forte, G., Tjaden, H., Yao, Y., Rastogi, S. *Polymer (Guildf)*., 2012, **53**,

- 2897–2907.
16. Smith, P., Chanzy, H., Rotzinger, B. *Polym. Commun.*, 1985, **26**, 258–260.
 17. Smith, P., Chanzy, H. D., Rotzinger, B. P. *J. Mater. Sci.*, 1987, **22**, 523–531.
 18. Rotzinger, B. P., Chanzy, H. D., Smith, P. *Polymer (Guildf.)*, 1989, **30**, 1814–1819.
 19. Tuskaev, V. A., Gagieva, S. C., Kurmaev, D. A., Kolosov, N. A., Mikhaylik, E. S., Golubev, E. K., Sizov, A. I., Zubkevich, S. V., Vasil'ev, V. G., Nikiforova, G. G., Buzin, M. I., Serenko, O. A., Bulychev, B. M. *Polymers (Basel)*, 2018, **10**, 1–13.
 20. Bando, Y., Chammingkwan, P., Terano, M., Taniike, T. *Macromol. Chem. Phys.*, 2018, **219**, 1–8.
 21. Namkajorn, M., Alizadeh, A., Romano, D., Rastogi, S., McKenna, T. F. L. *Macromol. React. Eng.*, 2016, **217**, 1521–1528.
 22. A. Alizadeh, M. Namkajorn, E. Somsook, T.F.L. McKenna, *Macromol. Chem. Phys.*, 2015, **216**, 903-913
 22. Vyazovkin, S., Sbirrazzuoli, N. *Macromol. Rapid Commun.*, 2004, **25**, 733–738.
 23. Vyazovkin, S. *Isoconversional Kinetics of Thermally Stimulated Processes*, Springer, 2015.
 24. Vyazovkin, S. *Phys. Chem. Chem. Phys.*, 2016, **18**, 18643–18656.
 25. Brem, A., Lhost, O., Tervoort, T. A. *Macromolecules*, 2020, **53**, 5957-5970.
 26. Hoffman, J. D., Miller, R. L. *Polymer (Guildf.)*, 1997, **38**, 3151–3212.
 27. Christakopoulos, F., Troisi, E. M., Sologubenko, A. S., Friederichs, N., Stricker, L., Tervoort, T. A. *Polymer (Guildf.)*, 2021, **222**, 123633.
 28. Lauritzen, J. I., Hoffman, J. D. *J. Chem. Phys.*, 1959, **31**, 1680–1681.
 29. Rastogi, S., Yao, Y., Ronca, S., Bos, J., Van Der Eem, J. *Macromolecules*, 2011, **44**, 5558–5568.
 30. Kanamoto, T., Tsuruta, A., Tanaka, K., Takeda, M., Porter, R. S. *Polym. J.*, 1983, **15**, 327–329.

31. Nooyen, G., Oostra, H. (DSM N.V.), WO 1993015118A1, 1993.
32. Friederichs, N., Gerlofsma, R. (Saudi Basic Industries Corp.), US 20110034650A1, 2011.
33. Lopes do Rosario, PhD Thesis, R. Université Claude Bernard Lyon, 2022.
34. Dashti, A., Mazloumi, S. H., Akbari, A., Ahadiyan, H. R., Emami, A. R. *J. Chem. Eng. Data*, 2016, **61**, 693–697.
35. Wunderlich, B., Cormier, C. M. *J. Polym. Sci. Part A-2 Polym. Phys.*, 1967, **5**, 987–988.
36. Scholte, T. G., Meijerink, N. L. J., Schoffeleers, H. M., Brands, A. M. G. *J. Appl. Polym. Sci.*, 1984, **29**, 3763–3782.
37. Kissinger, H. E. *Anal. Chem.*, 1957, **29**, 1702–1706.
38. Friedman, H. L. *J. Polym. Sci. Part C Polym. Symp.*, 1964, **6**, 183–195.
39. Vyazovkin, S. *Unified Kinet. Process.*, 1995, **28**, 95–101.
40. Christakopoulos, F., Troisi, E., Tervoort, T. A. *Polymers (Basel)*, 2020, **12**, 791.
41. Vyazovkin, S., Wight, C. A. *Int. Rev. Phys. Chem.*, 1998, **17**, 407–433.
42. Arrhenius, S. *Zeitschrift für Phys. Chemie*, 1889.
43. Vyazovkin, S., Sbirrazzuoli, N. *Macromol. Rapid Commun.*, 2006, **27**, 1515–1532.
44. H. Westfahl Jr, M.B. Cardoso, *J. Appl. Cryst.*, 2011, **44**, 1123.
45. Ryan, A. J., Bras, W., Mant, G. R., Derbyshire, G. E. *Polymer (Guildf)*, 1994, **35**, 4537–4544.
46. Ruland, W. *Acta Crystallogr.*, 1961, **14**, 1180–1185.
47. Mo, Z., Zhang, H. *J. Macromol. Sci. Part C*, 1995, **35**, 555–580.